A New Technique for Detecting Dental Diseases by using High Speed Artificial Neural Networks

Hazem M. El-Bakry

Faculty of Computer Science & Information Systems,
Mansoura University, EGYPT
E-mail: helbakry20@yahoo.com

Nikos Mastorakis

Department of Computer Science,
Military Institutions of University Education (MIUE) -
Hellenic Naval Academy, Greece

Abstract – In this paper, a new fast algorithm for dental diseases detection is presented. Such algorithm relies on performing cross correlation in the frequency domain between input image and the input weights of fast neural networks (FNNs). It is proved mathematically and practically that the number of computation steps required for the presented FNNs is less than that needed by conventional neural networks (CNNs). Simulation results using MATLAB confirm the theoretical computations. One of the limitations of Direct Digital Radiography (DDR) is noise. Some recent publications have indicated that Digital Subtraction Radiography (DSR) might significantly aid in the clinical diagnosis of dental diseases, once various clinical logistic problems limiting its widespread use have been over come. Noise in digital radiography may result from sources other than variation in projection geometry during exposure. Structure noise consists of all anatomic features other than those of diagnostic interest. Limitations of plain radiographs in detecting early, small bone lesions are also due to the presence of structure noise. This research work has been under - taken in an attempt to minimize structure noise in digital dental radiography by using digital subtraction radiography. By minimizing the structure noise, the validity of the digitized image in detecting diseases is enhanced.

Keywords— Direct digital radiography, structure noise, dental bone lesions, digital subtraction radiography, fast neural networks, cross correlation.

I. Introduction

DSR has been shown to provide increased diagnostic accuracy over conventional radiography in the detection of minute bone changes [1]. In DSR, a reference radiograph is turned into a positive image in the computer. After alignment, contrast and geometric correction, the reference radiograph (background image) is subtracted from a second follow–up radiograph (original image) [2-6]. The result is a decrease in structure noise, because all anatomic structures that do not change between radiographs are shown as neutral gray. Areas of bone loss or gain between examinations are shown in shades of dark or light gray, respectively. DSR is a highly sensitive and specific method for the detection of small bony changes in periodontitis which is a disease affecting the investing structures (periodontal structures) around any tooth (eg. lamina dura, periodental membrane space and alveolar bone) [7-12].

II. Background of Digital Subtraction Radiography

DSR is an electronic image processing technique that has been shown to be of greater diagnostic value in the qualitative and quantitative detection of small periodontal bone lesions than conventional radiography [13]. Subtraction radiography was introduced to dentistry in the early 1980s as a method to facilitate visualization of the areas of osseous loss or gain. The use of digital image processing techniques has improved the sensitivity of intraoral radiographs for the detection of small osseous changes in periodonties [9, 11]. The concept underlying subtraction radiography is simple. An image processing computer subtracts all unchanging structures from a set of 2 radiographs taken at 2 different examinations (a base line image and another follow up image). The result is a neutral gray background in the areas that have not changed. By convention, areas of bone gain are shown in shades of gray darker than the background and areas of bone loss appear lighter. The ability of clinicians to detect minute bony changes using subtraction radiography has been demonstrated by several authors using artificially induced lesions in the skulls [4, 14].

Clinicians were able to accurately identify lesions in which less than 6% bone had been removed in 90% of the cases. In separate experiments, clinicians were able to detect the presence of artificial lesions with sensitivity of 91.3% and were able to rule out lesions with specificity of 96.7% [15]. Other validation studies have been performed using experimental animals. Small hydroxyapatite chips were used to simulate osseous lesions, and a strong linear relationship was observed between the lesions size and mass calculated from subtraction radiographs and the actual chip size and mass [16,17]. These previous validation studies involved either skulls or anesthetized experimental animals.

III. Materials and Methods

Two dental images were included in this research. The difference between these two images f(x,y) and h(x,y) are expressed as:

$$g(x,y) = f(x,y) - h(x,y) \quad (1)$$

where f(x,y) is the original image with structure noise, h(x,y) is the background of original image which a reference image has a great gray level (bright pixels) produced from original image, g(x,y) is the resulted image which demonstrates differences between original and background image[18]. Equation (1) is obtained by computing the difference between all pairs of corresponding pixels from (f) and (h). The key usefulness of subtraction is the enhancement of differences between images.

One of the most commercially successful and beneficial uses of image subtraction is in the area of medical imaging called mask mode radiograph. In this case h(x,y), the mask, is an X–ray image of a region of patient's body captured by an intensified TV camera (instead of traditional X–ray film) located opposite an X–ray source. The procedure consists of injecting a contrast medium into the patient's blood stream, taking a series of images of the same anatomical region as h(x,y), and subtracting this mask from the series of incoming images after injection of the contrast medium. The net effect of subtracting the mask from each sample in the coming stream of TV images is that the areas that are different between f(x,y) and h(x,y) appear in the output image as enhanced detail. Because images can be captured at TV rates, this procedure in essence gives a movie showing how the contrast medium propagates through the various arteries in the area being observed [19].

In recent years, computed radiography (CR), which provides direct digital acquisition of X-ray images, has been developed and widely accepted. Conventional radiographs had problems in image data production and transfer, but a CR technique has resolved some of these limitations, although image quality apparently is inferior to that of conventional radiographs[20].

Digital subtraction radiography scheme was established for aligning clinical in vivo radiographs based on the implementations of an automatic geometric registration method and a contrast correction technique[21].

IV. Implementation of Subtraction Radiography Method

Digital image subtraction is a method for reducing the structure noise of normal anatomic detail. Therefore it increases the signal to noise ratio shown in Eq.1. By increasing the signal to noise ratio, the pathology should be made more evident to the human observer. Digital image subtraction has been applied to almost every disease process which affects dental hard tissues [24].

The dramatic improvement in diagnostic performance has been clearly demonstrated in numerous researches. A prerequisite for digital subtraction radiography is that the projections should be identical or almost identical at the different examinations. Other prerequisites for subtraction are the ability to properly align the two images, this is refered to as registration, and the ability to correct for variations associated with exposure and processing that would obscure the changes in radiographic density associated with the pathology.

This prerequisite has limited the direct clinical application of this technique. Recent developments in reproducible radiographic techniques and gamma correction algorithms may provide the answers to these limitation. The application of longitudinal radiographic assessment techniques such as subtraction radiography may hold the greatest promise for improving diagnostic accuracy. Optical density of radiographs was digitized into gray levels using a drum–scanning microdensitometer with high accuracy [22]. Digital subtraction radiography requires close matching of the contrast in the films to be subtracted. Subtraction radiography is a potentially powerful method for monitoring the results of periodontal therapy. Its successful application in longitudinal studies requires that the variations caused by uncontrolled changes of X-ray imaging geometry, as well as by film exposure and processing conditions, be small relative to the changes of diagnostic interest occurring over the observation interval.

While these pre-requisites are difficult to attain, controlled studies have demonstrated that geometrical registrations using occlusal templates result in detectability of periodontal lesions that is significantly improved over conventional radiographic methods [23]. Reproducibility of film contrast can be maintained by electronic control of exposure time, X-ray tube current and voltage wave forms, and by careful film processing with quality control of the chemicals. Despite these efforts, contrast discrepancies do occur in practice.

Matlab program of subtraction radiograph was used to execute the subtraction between original image f(x,y) and background of original image h(x,y). The results of the present research are shown in figures (1-6). Fig. 1 shows insertion of the original image in '' Matlab program'', Fig. 3 represents the background of the original image, Figures 2, 4, and 6 show histograms of the original image, background and final image respectively. Fig. 5 represents the final subtracted image. From these figures, it could be noticed that the characteristics of the original image were significantly enhanced after subtraction

regarding visual characteristics as clarity, contrast, sharpness and resolution. Detection of early bone diseases or early subtle dental diseases was one of the major problems facing dental clinicians before the advent of DDR and DSR. Before DSR, Bone destruction cannot be detected on the dental radiograph before 50 – 60% de – mineralization occurs. DSR presents a highly sensitive diagnostic imaging modality that enhances the detection of early bone changes due to its high clarity.

V. Fast Dental Diseases Detection by using Neural Networks and Cross Correlation in the Frequency Domain

First neural networks are trained to classify sub-images which contain diseases from those which do not and this is done in the spatial domain. In the test phase, each sub-image in the input image (under test) is tested for the presence or absence of diseases. At each pixel position in the input image each sub-image is multiplied by a window of weights, which has the same size as the sub-image. This multiplication is done in the spatial domain. The outputs of neurons in the hidden layer are multiplied by the weights of the output layer. When the final output is high this means that the sub-image under test contain diseases and vice versa. Thus, we may conclude that this searching problem is cross correlation in the spatial domain between the image under test and the input weights of neural networks.

In this section, a fast algorithm for detecting diseases based on two dimensional cross correlations that take place between the tested image and the sliding window (20x20 pixels) is described. Such window is represented by the neural network weights situated between the input unit and the hidden layer. The convolution theorem in mathematical analysis says that a convolution of *f* with *h* is identical to the result of the following steps: let *F* and *H* be the results of the Fourier transformation of f and h in the frequency domain. Multiply *F* and *H* in the frequency domain point by point and then transform this product into spatial domain via the inverse Fourier transform [27]. As a result, these cross correlations can be represented by a product in the frequency domain. Thus, by using cross correlation in the frequency domain a speed up in an order of magnitude can be achieved during the detection process [25].

In the detection phase, a sub-image *X* of size *mxz* (sliding window) is extracted from the tested image, which has a size *P*x*T*, and fed to the neural network. Let W_i be the vector of weights between the input sub-image and the hidden layer. This vector has a size of *mxz* and can be represented as *mxz* matrix. The output of hidden neurons h_i can be calculated as follows:

$$h_i = g\left(\sum_{j=1}^{m} \sum_{k=1}^{z} W_i(j,k)X(j,k) + b_i \right) \quad (2)$$

where *g* is the activation function and b_i is the bias of each hidden neuron *(i).* Eq.2 represents the output of each hidden neuron for a particular sub-image *I*. It can be computed for the whole image Ψ as follows:

$$h_i(u,v) = g\left(\sum_{j=-m/2}^{m/2} \sum_{k=-z/2}^{z/2} W_i(j,k)\Psi(u+j,v+k) + b_i \right) \quad (3)$$

Eq.(3) represents a cross correlation operation. Given any two functions *f* and *g*, their cross correlation can be obtained by [26]:

$$g(x,y) \otimes f(x,y) = \left(\sum_{m=-\infty}^{\infty} \sum_{z=-\infty}^{\infty} g(m,z) f(x+m,y+z) \right) \quad (4)$$

Therefore, Eq.(3) can be written as follows [25]:

$$h_i = g\left(W_i \otimes \Psi + b_i \right) \quad (5)$$

where h_i is the output of the hidden neuron *(i)* and h_i *(u,v)* is the activity of the hidden unit *(i)* when the sliding window is located at position *(u,v)* in the input image Ψ and $(u,v) \in [P-m+1, T-n+1]$.
Now, the above cross correlation can be expressed in terms of the Fourier Transform:

$$W_i \otimes \Psi = F^{-1}\left(F(\psi) \bullet F^*\left(W_i \right) \right) \quad (6)$$

(*) means the conjugate of the *FFT* for the weight matrix. Hence, by evaluating this cross correlation, a speed up ratio can be obtained comparable to conventional neural networks. Also, the final output of the neural network can be evaluated as follows:

$$O(u,v) = g\left(\sum_{i=1}^{q} W_O(i)\, h_i(u,v) + b_O \right) \quad (7)$$

where *q* is the number of neurons in the hidden layer. *O(u,v)* is the output of the neural network when the sliding window located at the position *(u,v)* in the input image Ψ. W_o is the weight matrix between hidden and output layer.

The complexity of cross correlation in the frequency domain can be analyzed as follows:

1. For a tested image of *NxN* pixels, the *2D-FFT* requires a number equal to $N^2 log_2 N^2$ of complex computation steps. Also, the same number of complex computation steps is required for computing

the *2D-FFT* of the weight matrix for each neuron in the hidden layer.

2. At each neuron in the hidden layer, the inverse *2D-FFT* is computed. So, *q* backward and *(1+q)* forward transforms have to be computed. Therefore, for an image under test, the total number of the *2D-FFT* to compute is $(2q+1)N^2 log_2 N^2$.

3. The input image and the weights should be multiplied in the frequency domain. Therefore, a number of complex computation steps equal to qN^2 should be added.

4. The number of computation steps required by the fast neural networks is complex and must be converted into a real version. It is known that the two dimensional Fast Fourier Transform requires $(N^2/2)log_2 N^2$ complex multiplications and $N^2 log_2 N^2$ complex additions [26]. Every complex multiplication is realized by six real floating point operations and every complex addition is implemented by two real floating point operations. So, the total number of computation steps required to obtain the *2D-FFT* of an *NxN* image is:

$$\rho=6((N^2/2)log_2 N^2) + 2(N^2 log_2 N^2) \quad (8)$$

which may be simplified to:

$$\rho=5N^2 log_2 N^2 \quad (9)$$

Performing complex dot product in the frequency domain also requires $6qN^2$ real operations.

5. In order to perform cross correlation in the frequency domain, the weight matrix must have the same size as the input image. Assume that the input object has a size of (nxn) dimensions. So, the search process will be done over sub-images of (nxn) dimensions and the weight matrix will have the same size. Therefore, a number of zeros = (N^2-n^2) must be added to the weight matrix. This requires a total real number of computation steps = $q(N^2-n^2)$ for all neurons. Moreover, after computing the *2D-FFT* for the weight matrix, the conjugate of this matrix must be obtained. So, a real number of computation steps $=qN^2$ should be added in order to obtain the conjugate of the weight matrix for all neurons. Also, a number of real computation steps equal to *N* is required to create butterflies complex numbers $(e^{-jk(2\Pi n/N)})$, where $0<K<L$. These *(N/2)* complex numbers are multiplied by the elements of the input image or by previous complex numbers during the computation of the *2D-FFT*. To create a complex number requires two real floating point operations. So, the total number of computation steps required for the fast neural networks becomes:

$$\sigma=(2q+1)(5N^2 log_2 N^2) +6qN^2+q(N^2-n^2)+qN^2 +N \quad (10)$$

which can be reformulated as:

$$\sigma=(2q+1)(5N^2 log_2 N^2) +q(8N^2-n^2) +N \quad (11)$$

6. Using a sliding window of size nxn for the same image of *NxN* pixels, $q(2n^2-1)(N-n+1)^2$ computation steps are required when using traditional neural networks for object detection process. The theoretical speed up factor η can be evaluated as follows:

$$\eta=\frac{q(2n^2-1)(N-n+1)^2}{(2q+1)(5N^2 log_2 N^2)+q(8N^2-n^2)+N} \quad (12)$$

The theoretical speed up ratio Eq. 12 with different sizes of the input image and different in size weight matrices is listed in Table 1. Practical speed up ratio for manipulating images of different sizes and different in size weight matrices is listed in Table 2 using 2.7 GHz processor and *MATLAB ver 5.3*. An interesting property with FNNs is that the number of computation steps does not depend on either the size of the input sub-image or the size of the weight matrix (n). The effect of (n) on the number of computation steps is very small and can be ignored. This is in contrast to CNNs in which the number of computation steps is increased with the size of both the input sub-image and the weight matrix (n).

In practical implementation, the multiplication process consumes more time than the addition one. The effect of the number of multiplications required for conventional neural networks in the speed up ratio (Eq.12) is more than the number of of multiplication steps required by the FNNs. In order to clear this, the following equation (η_m) describes relation between the number of multiplication steps required by conventional and FNNs:

$$\eta_m=\frac{qn^2(N-n+1)^2}{(2q+1)(3N^2 log_2 N^2)+6qN^2} \quad (13)$$

The results listed in Fig. 7 prove that the effect of the number of multiplication steps in case of CNNs is more than FNNs and this the reason why practical speed up ratio is larger than theoretical speed up ratio.

For general fast cross correlation the speed up ratio (η_g) is in the following form:

$$\eta_g=\frac{q(2n^2-1)N^2}{(2q+1)(5(N+\tau)^2 log_2(N+\tau)^2)+q(8(N+\tau)^2-n^2)+(N+\tau)} \quad (14)$$

where τ is a small number that depends on the size of the weight matrix. General cross correlation means that the process starts from the first element in the input matrix. The theoretical speed up ratio for general fast cross correlation (η_g) defined by Eq.(14) is shown in Fig. 8. Compared with *MATLAB* cross correlation function *(xcorr2)*, experimental results

show that the proposed algorithm is faster than this function as shown in Fig. 9.

VI. Conclusion

A new fast algorithm for dental diseases detection has been presented. This has been achieved by performing cross correlation in the frequency domain between input image and the input weights of fast neural networks (FNNs). It has been proved mathematically and practically that the number of computation steps required for the presented FNNs is less than that needed by conventional neural networks (CNNs). Simulation results using MATLAB has confirmed the theoretical computations. In addition, it has been shown that digital subtraction radiography increases diagnostic accuracy over digital radiography with structure noise. Minimizing structure noise is an important contribution in accurate diagnosis of oral pathological lesions. The human errors inherent with visual interpretation of dental diseases from images will be minimum due to increasing the image characteristics after noise removal. This is a step forward in achieving accurate diagnosis as well as increasing the utility of digitized radiographs in providing qualitative and quantitative information concerning the investigated diseases.

References

[1] Reddy, MS., Bruch, JM., Jeffcoat, MK., and Williams, RC.: Contrast enhancement as an aid to interpretation in digital subtraction radiography, Oral Surg Oral Med Oral pathol, vol. 71, 1991, pp. 763 – 769.

[2] Grondahl, k., Grondahl, H. and Webber, RL.: Digital subtraction radiography for diagnosis of periodontal bone lesions with simulated high speed systems, Oral Surg Oral Med Oral Pathol, vol. 55, 1983, pp. 313-318.

[3] Hausmann, E., Christersson, L., Dunford,R., Wikesjo,U. and enco,R.J.: Usefulness of subtraction radiography in the evaluation of periodontal therapy, J Periodontol, vol. 1, 1985, pp. 4-7,.

[4] Ortman, LM., Dunford, R., McHenry, k. and Hausmann, E.: Subtraction radiography and computer assisted densitometric analysis of standardized radiographs, J Periodont Res, vol. 20, 1986, pp. 644-651.

[5] Rethman,M., Ruttimann, U. and O'neal, R.: Diagnosis of bone lesions by subtraction radiography, J Periodontol. vol. 56, 1985, pp. 324-328.

[6] Ruttimann, U.E. and Webber, RL.: Volumetry of localized bone lesions by subtraction radiography, J Periodont Res, vol. 22, 1987, pp. 215-226.

[7] Bragger, D., pasquali, L., Rylander, H., Carnes, D. and Kornman, K.S.: Computer–assisted densitometric image analysis in periodontal radiography: a methological study, J Cline Periodontol, vol. 15, 1988, pp. 27-37.

[8] Grondahl, H., Grondhahl, K. and Webber, R.L.: A digital subtraction technique for dental radiography, Oral Surg Oral Med Oral Pathol, vol. 55, 1983, pp. 96-102.

[9] Grondahl, H.G. and Grondahl, K.: Subtraction radiography for the diagnosis of Periodontal bone lesions, Oral Surg Oral Med Oral Pathol, vol. 55, 1983, pp. 208-213.

[10] Grondahl, K., Grodahl, H. and Webber, R.L.: Influence of variations in projection geometry on the detectability of periodontal bone lesions, J Clin Periodontal, vol. 11, 1984, pp. 411-420.

[11] Webber, R.L., Ruttimann, U.E. and Grondahl, H.G.: X-ray image subtraction as a basis for assessment of periodontal changes, J periodont Res. vol. 17, 1982, pp. 609-611.

[12] Revez, G., Kundel, H. and Graber, M.A.: The influence of structured noise on the detection of radiologic abnormalities, Invest Radiol, vol. 9, pp. 479-486, 1974.

[13] Jeffcoat, MK., Reddy, MS., Magnusson, L., Johnson, B., Mecedith, MP. and Cavanaugh, Jr.: Efficacy of quantitive digital subtraction radiography using radiographs exposed in Multicenter trial, Journal of Periodontal Research. vol. 31, 1996, pp. 157 – 160.

[14] Jeffcoat, M.K., Reddy, M.S. And Jeffcoat, R.L.: A morphologically aided technique for quantitative subtraction of dental radiographic images, IEEE/EMBS. vol. 12, 1990, pp. 2068-2070.

[15] Jeffcoat, M.K., Page, R., Reddy, M.S., Wannawisote, A., Wait, P., Palcanis, k. and Cogen, R.: Use of digital radiography to demonstrate the potential of naproxen as an adjust in the treatment of rapidly progressive periodontities, J periodont Res, vol. 26, 1991, pp. 415-421.

[16] Jeffcoat, M.K., Reddy, MS.: Digital subtraction radiography for longitudinal assessment of peri-implant bone change: method and validation, Adv Dent Res. vol. 7, 1993, pp. 196-201.

[17] Jeffcoat, M.K., Reddy, M.S., Webber, RL., Wiliams, R.S. and Ruttimann, U.E.: Extraoral control of geometry for digital subtraction radiography, J Periodont Res. v. 22, 1987, pp. 396-402.

[18] Gotfredsen, E., Wenzel, A. and Grondahl, HG.: Observes use of image enhancement in assessing caries in radiographs taken by four intra-oral digital systems, Dentomaxillofac, Radiol, vol. 25, no. 1, 1996, pp. 34-38.

[19] Nakagawa, K., Mizuno, S., Aoki, Y., and Ohtomo, K.: C-MOS Flat-panel sensor for real-time X-ray imaging. Radiarion Medicine, vol. 18, no. 6, 2000, pp. 349-354.

[20] Zacharaki, E.I., Matsopoulos, G.K., Asvestas, P.A., Nkita, K.S., Grondahl, K. and Grondahl, H.G.: Digital subtraction radiography secheme based on automatic multiresolution registration, Dentomaxillofacial Radiology, vol. 33, 2004, pp. 379-390,.

[21] Akdeniz, BG. and Sogur, E.: An ex vivo comparison of conventional and digital radiography for perceived image quality of root fillings, International Endodontic Journal, vol. 38, 2005, pp. 397-401.

[22] Ohki, M., Okano, T. and Yamada, N.: A contrast – correction method for digital subtraction method for digital subtraction radiography, Journal of Periodontal Research, vol. 23, 1988, pp. 277 – 280.

[23] Ruttimann, E., Richard, L. and Schmidt, E.: A robust digital method for film contrast correction in subtraction radiography, Journal of eriodontal Research, vol. 21, 1986, pp. 486 – 495.

[24] Anis Ebrahim, N. M., Minimizing Structure Noise In Digital Dental Radiography, Phd Thesis, Cairo university, Egypt, 2008.

[25] El-Bakry, H. M., "New Faster Normalized Neural Networks for Sub-Matrix Detection using Cross Correlation in the Frequency Domain and Matrix Decomposition," Applied Soft Computing journal, vol. 8, issue 2, March 2008, pp. 1131-1149.

[26] Cooley, J. W. and Tukey, J. W., "An algorithm for the machine calculation of complex Fourier series," Math. Comput. 19, 1965, pp. 297–301.

[27] Klette R., and Zamperon, "Handbook of image processing operators, " John Wiley & Sonsltd, 1996.

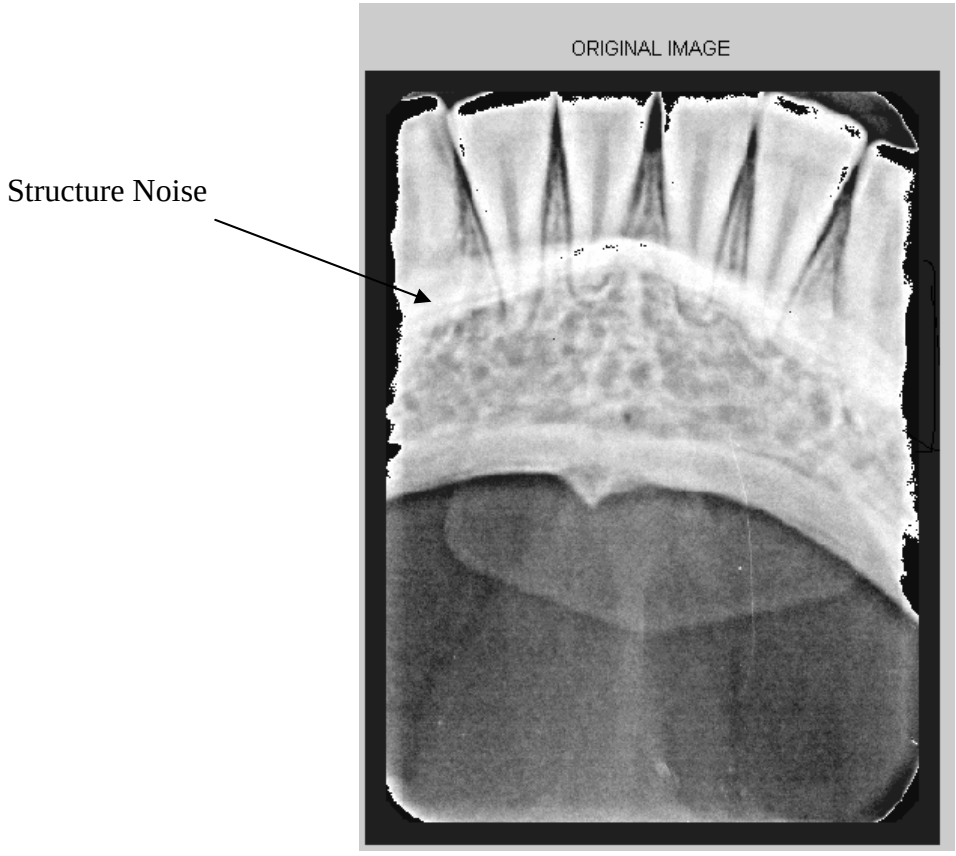

Fig. 1. Original image with structure noise.

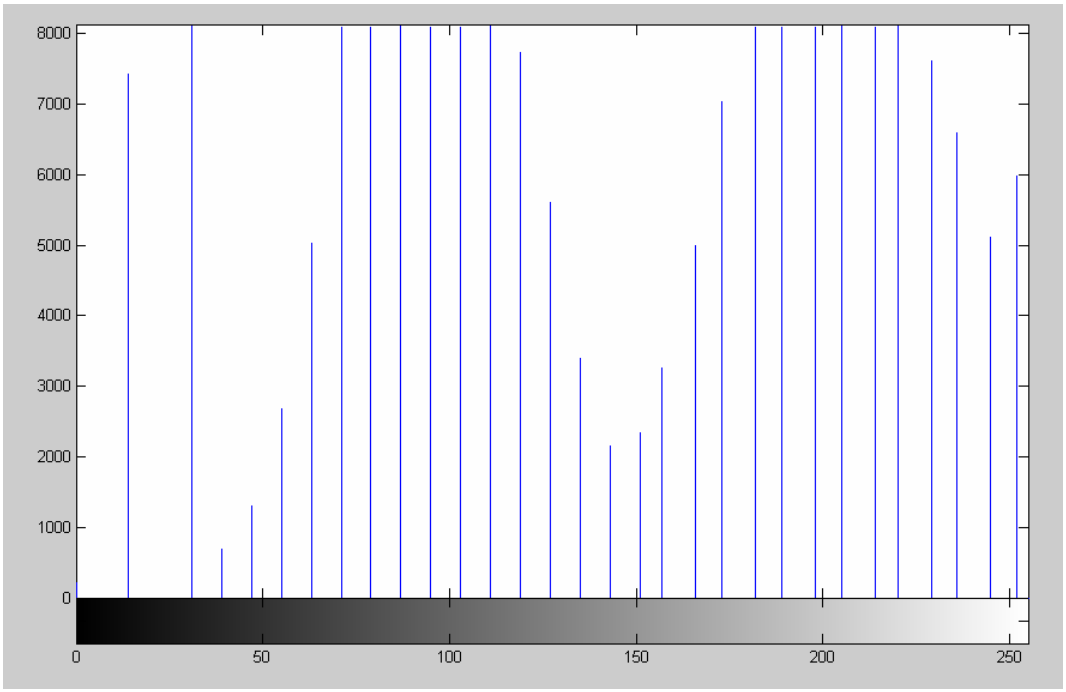

Fig. 2. Histogram of the original image.

Fig. 3. Background of the original image.

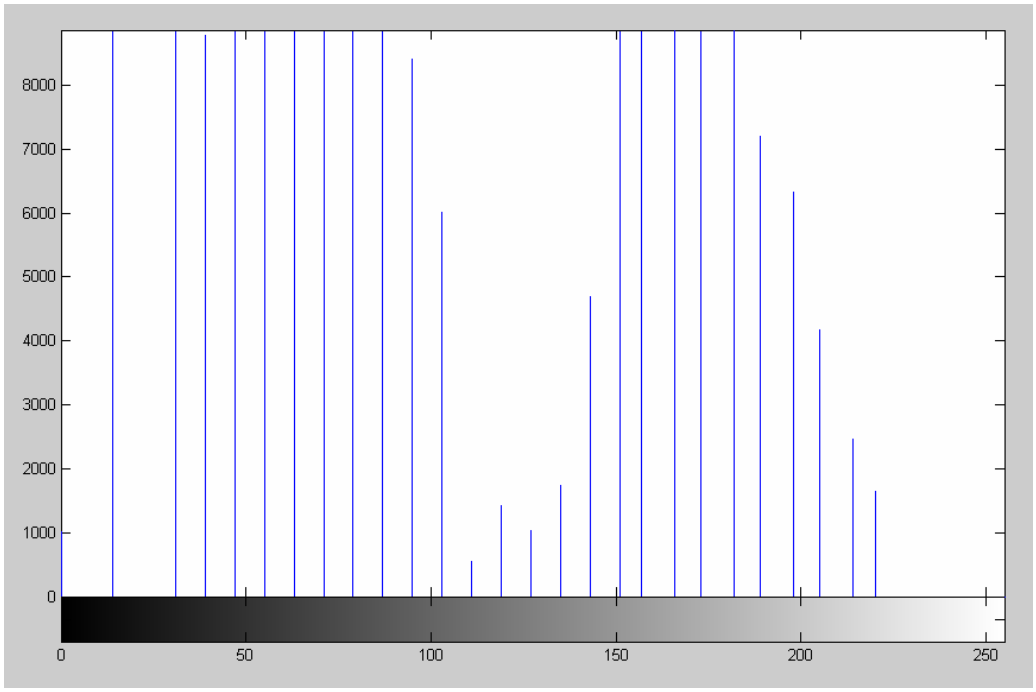

Fig. 4. Histogram of background of the original image.

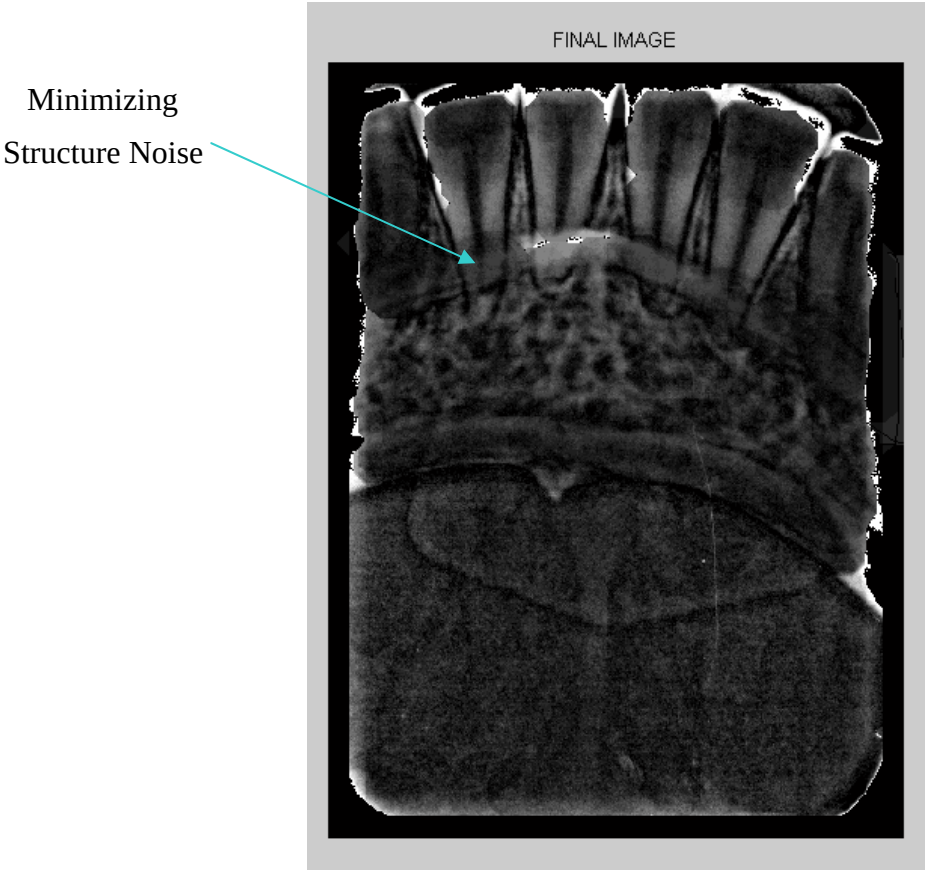

Fig. 5. Final image of the original image with minimized structure noise.

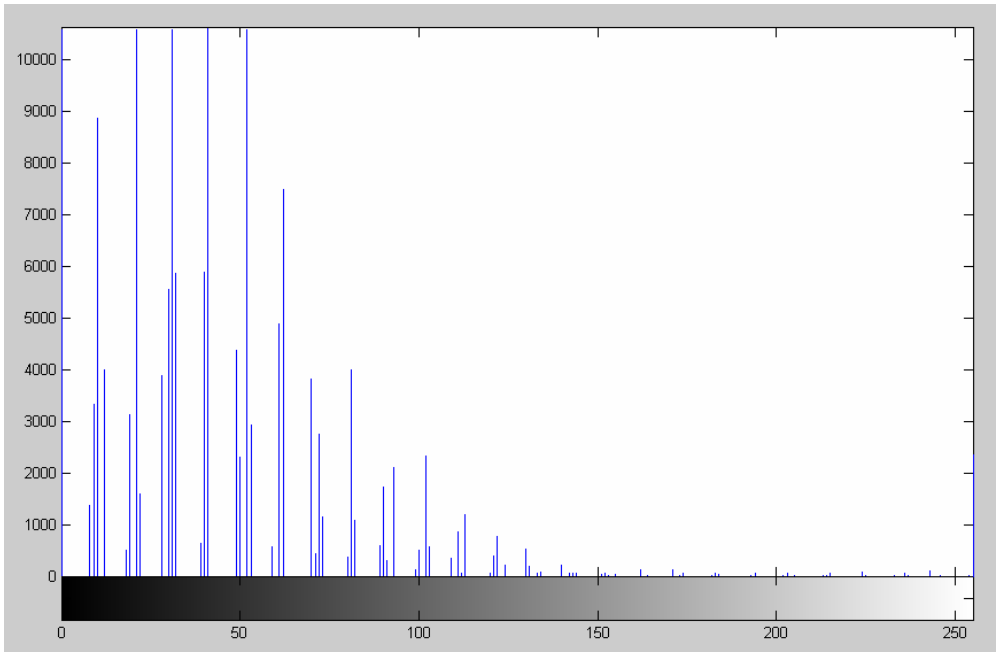

Fig. 6. Histogram of the final image.

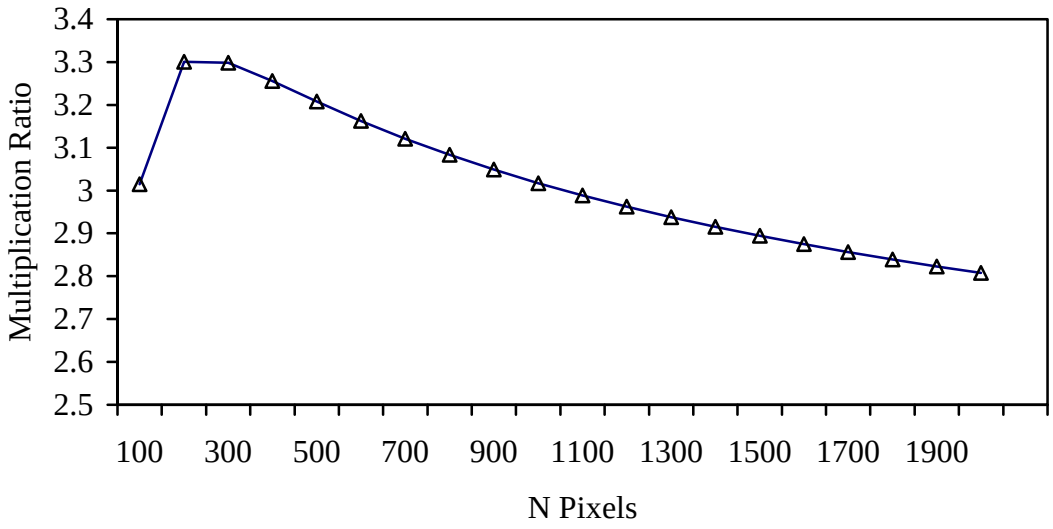

Fig. 7. A comparison between the number of multiplication steps required for CNNs and FNNs to manipulate images with different sizes (n=20, q=30).

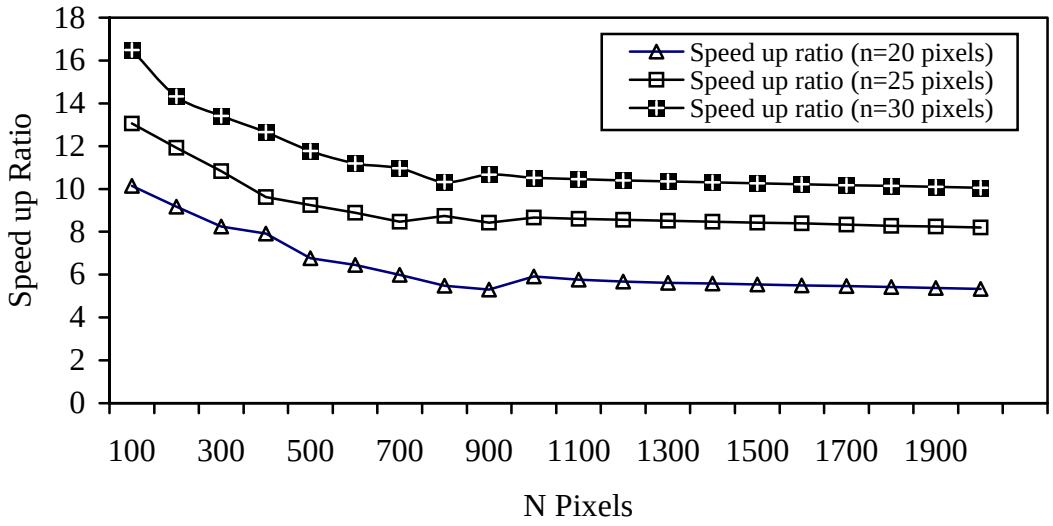

Fig. 8. The theoretical speed up ratio for the general faster cross correlation algorithm.

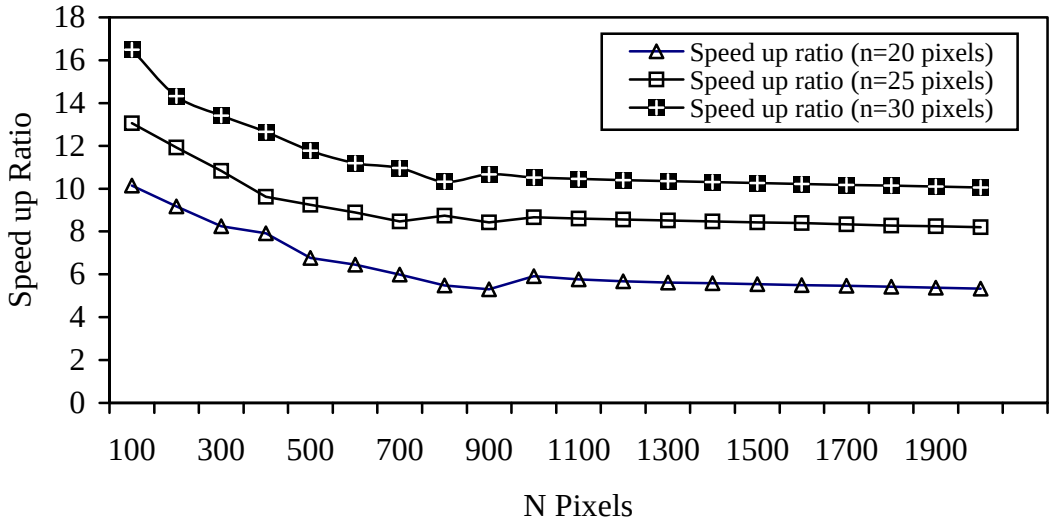

Fig. 9. Simulation results of the speed up ratio for the general faster cross correlation compared with the MATLAB cross correlation function (XCORR2).

Table 1
The Theoretical Speed up Ratio for Images with Different Sizes.

Image size	Speed up ratio (n=20)	Speed up ratio (n=25)	Speed up ratio (n=30)
100x100	3.67	5.04	6.34
200x200	4.01	5.92	8.05
300x300	4.00	6.03	8.37
400x400	3.95	6.01	8.42
500x500	3.89	5.95	8.39
600x600	3.83	5.88	8.33
700x700	3.78	5.82	8.26
800x800	3.73	5.76	8.19
900x900	3.69	5.70	8.12
1000x1000	3.65	5.65	8.05
1100x1100	3.62	5.60	7.99
1200x1200	3.58	5.55	7.93
1300x1300	3.55	5.51	7.93
1400x1400	3.53	5.47	7.82
1500x1500	3.50	5.43	7.77
1600x1600	3.48	5.43	7.72
1700x1700	3.45	5.37	7.68
1800x1800	3.43	5.34	7.64
1900x1900	3.41	5.31	7.60
2000x2000	3.40	5.28	7.56

Table 2
Practical Speed up Ratio for Images with Different Sizes using MATLAB Ver 5.3.

Image size	Speed up ratio (n=20)	Speed up ratio (n=25)	Speed up ratio (n=30)
100x100	7.88	10.75	14.69
200x200	6.21	9.19	13.17
300x300	5.54	8.43	12.21
400x400	4.78	7.45	11.41
500x500	4.68	7.13	10.79
600x600	4.46	6.97	10.28
700x700	4.34	6.83	9.81
800x800	4.27	6.68	9.60
900x900	4.31	6.79	9.72
1000x1000	4.19	6.59	9.46
1100x1100	4.24	6.66	9.62
1200x1200	4.20	6.62	9.57
1300x1300	4.17	6.57	9.53
1400x1400	4.13	6.53	9.49
1500x1500	4.10	6.49	9.45
1600x1600	4.07	6.45	9.41
1700x1700	4.03	6.41	9.37
1800x1800	4.00	6.38	9.32
1900x1900	3.97	6.35	9.28
2000x2000	3.94	6.31	9.25